IPP-Report

Max-Planck-Institut für Plasmaphysik

H. Wobig, T. Andreeva, C. D. Beidler, E. Harmeyer, F. Herrnegger, J. Kißlinger, M. Köppen, F. Schauer

On Coil Systems of Optimized Stellarator Reactors

IPP 14/1
Dezember, 2009

On Coil Systems of Optimized Stellarator Reactors

H. Wobig, T. Andreeva, C.D. Beidler, E. Harmeyer, F. Herrnegger,
J. Kißlinger, M. Köppen, F. Schauer
Max-Planck-Institut für Plasmaphysik, Garching bei München, EURATOM-Ass.

Abstract

Superconducting modular coils are the main technical components of the stellarator experiment Wendelstein 7-X in the city of Greifswald (Germany). An analytic description of the coils by 5 segments of cubic Bézier curves allows one to represent the Wendelstein 7-X coils accurately and to scale-up the coils to reactor dimensions. By varying the control points of the Bézier curves the impact of modifications on the structure of the magnetic surfaces can be easily investigated. Keeping the Wendelstein 7-X coil shape invariant, configurations with 5, 4 and 3 field periods have been studied. In all cases the coils are roughly 4 times larger than Wendelstein 7-X coils. The code MODUCO represents the coil system on the screen and allows an interactive modification of the coils followed by a computation of magnetic surfaces and magnetic induction inside the coils. Thus, engineering and physics constraints can be addressed simultaneously.

1 Introduction

Stellarator reactor studies in Europe were initiated by A. Gibson at al. [**?**] who analysed a classical $\ell = 3$-stellarator and its reactor prospects. The classical stellarator consists of a set of toroidal field coils and helical windings providing rotational transform. These helical windings are located inside the TF coils, which obviously presents some obstacles to the construction and assembly of the device. A particular disadvantage of the classical stellarator configuration is caused by the interaction of the toroidal field coils and the helical windings. Since the helices are imbedded in a large toroidal magnetic field, large radial forces occur, which alternate in direction from one helix to the next. Thus, for large devices with significant confining fields, the problem of supporting the helices turnes out to be very serious, as relatively little space is available for structural material. As a responce to this issue the concept of modular stellarators was developed during the design phase of Wendelstein 7-A [**?**].

The term modular stellarator refers to a generalized stellarator configuration with nested magnetic surfaces achieved by a system of discrete coils which provide both toroidal and poloidal fields. Since there is no net toroidal current, no vertical field coils are needed. A modular stellarator, therefore, has no continuous helical windings; all coils are closed poloidally. Furthermore, there is no force pointing towards the minor axis "inside" modular coils. Thus the support structure can be located outside and between the coils.

Modular coils offer a chance to realize a large variety of stellarator configurations, limiting the stray magnetic fields outside the machine to a negligible level. In particular, this refers to the superposition of helical fields with different toroidally variable helicity and mirror fields, which is desirable in the search for optimum configurations. Here optimisation entails a choice of rotational transform and plasma shaping with respect to optimum plasma equilibrium, stability and neoclassical confinement. A further advantage of modular coils is a more practical one: modular coils need not be manufactured at the reactor site as their size and weight are small

enough to allow conventional shipping. They can also be tested before being installed into the reactor core thus minimizing the risk of failure during operation.

The vacuum field was the starting point in the first stellarator concepts, however in designing the Wendelstein 7-X stellarator another procedure has been applied. This method starts from a plasma equilibrium and computes the coil system afterwards using the NESCOIL code developed by P. Merkel [**?**]. In optimised stellarators, however, the vacuum field and the finite-beta equilibrium differ only slightly and therefore optimisation of stellarator equilibria can already be done by shaping the vacuum field properly and regarding the results of equilibrium codes as a guide-line. In the following we present a new method to model modular coils in terms of cubic Bézier curves. This allows one to represent a large spectrum of coil shapes with a fixed number of parameters. The coils can be modelled interactively on a PC followed by a quick computation of the vacuum field inside and outside the coils. Engineering constraints can be included thus combining technical and physics principles of optimisation.

The present paper describes the code MODUCO (MODUlar COils) and discusses various examples of coil configurations and their reactor prospects. The code is written in C^{++} and utilizes OpenGL for graphic display. Input data are menu-controlled allowing a quick and interactive handling of data and display.

2 Geometry of modular coils

The basic principle of representing modular coils is as follows: the core of the coil is a closed curve, which is called the central filament. The central filament consists of several segments which are described by analytic curves. Starting from a cylindrical coordinate system Fourier series of a coil shape in the poloidal angle seem to be the natural approach to represent the non-circular and non-planar coils. However, if the shape of the coils is rather complex a large number of Fourier coefficients is required. The correlation between the Fourier coefficients and the shape is difficult to understand and the variation of one or several coeffcients may change the whole shape of the coils. Cubic spline approximation [**?**] is a way out of this dilemma since a fixed number of points in space - the control points - are sufficient to model complex coils. In general, however, none of the control points are located on the coils which may be inconvenient in modelling the coils interactively,

In the procedure described in this paper a segment of the central filament is represented by a cubic Bézier curve with a continuous tangent vector. A Bézier curve is defined by four points in space P_1, P_2, P_3, P_4 where P_1 and P_4 are the endpoints of the curve and P_2, P_3 define the tangent vector at the endpoints. A minimum of four such Bézier segments is needed to represent a closed modular coil. Increasing the number of segments allows one to represent any coil shape. However, five segments seem to be sufficient to model stellarator reactor coils.

The general procedure is as follows: we define N coil points $\boldsymbol{X}_i,\ i = 1, ...; N$ and N control points $\boldsymbol{Q}_i,\ i = 1, ..., N$. The vector $\boldsymbol{Q}_i - \boldsymbol{X}_i$ defines the tangent vector at the coil point $\boldsymbol{X}_i$. With $d_i = |\boldsymbol{Q}_i - \boldsymbol{X}_i|$ the tangent unit vector is $\boldsymbol{t}_i = (\boldsymbol{Q}_i - \boldsymbol{X}_i)/d_i$. A second set of control points is defined by $\boldsymbol{Q}'_i = 2\boldsymbol{X}_i - \boldsymbol{Q}_i$. This completes the number of points characterising the central filament and any segment of the central filament is fixed by the points $\boldsymbol{X}_i, \boldsymbol{X}_{i+1}, \boldsymbol{Q}_i, \boldsymbol{Q}'_{i+1}$. Given a parameter $t,\ 0 \le t \le 1$ the representation of the segment is

$$\boldsymbol{Y}_i(t) = (1-t)^3\boldsymbol{X}_i + 3t(1-t)^2\boldsymbol{Q}_i + 3t^2(1-t)\boldsymbol{Q}'_{i+1} + t^3\boldsymbol{X}_{i+1} \tag{1}$$

This cubic Bézier curve connects the two points $\boldsymbol{X}_i$ and $\boldsymbol{X}_{i+1}$: $\boldsymbol{Y}_i(0) = \boldsymbol{X}_i$, $\boldsymbol{Y}_i(1) = \boldsymbol{X}_{i+1}$. In this version the segments $\boldsymbol{Y}_i$ and $\boldsymbol{Y}_{i+1}$ join at $\boldsymbol{X}_{i+1}$ with a continuous tangent vector and continuous curvature. A more general alternative is to restrict the continuity to the tangent vector only and make the curvature discontinuous. This allows one to model, for example,

D-shaped tokamak coils although a sufficient approximation to D-shaped coils is also possible with continuous curvature. The advantage of Bézier curves is the fact that the points $\boldsymbol{X}_i$

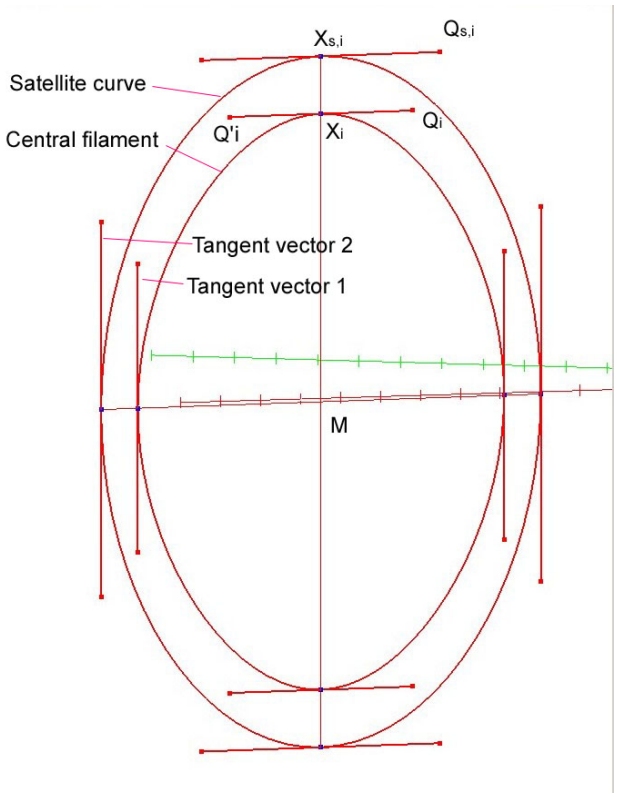

Figure 1: Scheme of a modular coil. Central filament and satellite curve

are the endpoints of the segments and therefore specifying these points already yields a rough approximation of the coils. In particular, this is helpful in modelling coils interactively on a PC. It was found that four segments ($N = 4$) are sufficient to model a large class of coil shapes like D-shaped tokamak coils, $\ell = 2$-stellarator coils. Modular coils of a Helias-type stellarator, however, needs five segments for proper modelling. If a more complex coil geometry is required the number of segments can be extended to more than five.

2.1 Definition of the normal vector

The derivative $\boldsymbol{Y}_i'(t)$ yields the tangent vector $\boldsymbol{t}_i = \boldsymbol{Y}_i'(t)/|\boldsymbol{Y}_i'(t)|$ of the central filament while there is an ambiguity in defining the normal vector. The normal vector determines the orientation of the winding pack and the coil casing. A straightforward method would be to use the natural coordinate system of the segments defined by the normal and binormal vector of the segments. However, this method fixes also the torsion of the coil. If the coils deviate strongly from planar geometry this natural torsion may be too large and not practicable for engineering reasons.

We define the normal vector of the coil in a different way which allows one to account for technical restrictions. For this purpose we introduce the center $\boldsymbol{M}$ of the coil as the average of the coil points $\boldsymbol{X}_i$: $\boldsymbol{M} = \sum \boldsymbol{X}_i/N$ and define the local radius of the coil $r_i(t) = |(\boldsymbol{Y}_i(t) - \boldsymbol{M})|$. The normal vector of the coil is given by $\boldsymbol{n}_i = (\boldsymbol{Y}_i(t) - \boldsymbol{M})/r_i$ and the binormal by $\boldsymbol{b}_i = \boldsymbol{t}_i \times \boldsymbol{n}_i$. Normal and binormal vector define the plane of the coil cross section. This coordinate system will be designated system 1.

This method does not account for the position and orientation of the neighbouring coils.

Since in those regions where the coils are close to each other further adjustments of the the coils may be necessary, we introduce another parameter, which allows to tilt the normal vector in regions where it is required. For this purpose we start from system 1 and define a new normal and binormal vector at the coil points $\boldsymbol{X}_i$. Every coil point $\boldsymbol{X}_i$ has a satellite point $\boldsymbol{X}_{s,i}$ and a control point $\boldsymbol{Q}_{s,i}$. The new system, called system 2, is obtained by rotating the base vectors in the plane of the coil cross section. Connecting the endpoints $\boldsymbol{X}_{s,i}$ of the new normal vector by a cubic interpolation leads to a second closed curve in space, the satellite curve, which allows us to construct the normal vector (and binormal vector) at every point of the coils. In summary, by fixing the coil geometry at the coil points $\boldsymbol{X}_i$ all other coil points are found by cubic interpolation. The flexibility of this method is sufficient to represent any modular coil

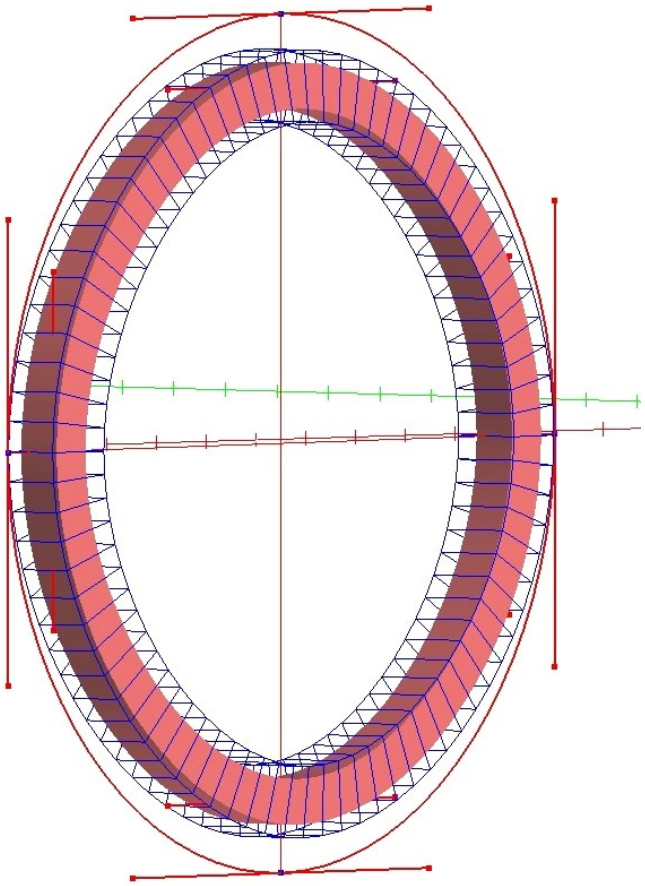

Figure 2: Modular coil, winding pack and coil case (wire frame). Furthermore, the satellite curve is shown which defines the orientation of the coil cross section

system. The next figure **??** shows a non-planar coil. The figure on the right side indicates how the coil cross section has been tilted. A simple modification of the circular coil is a planar D-shaped coil in tokamak configurations. This is a non-planar coil, the toroidal excursion of the coil can be used to generate a vertical field.

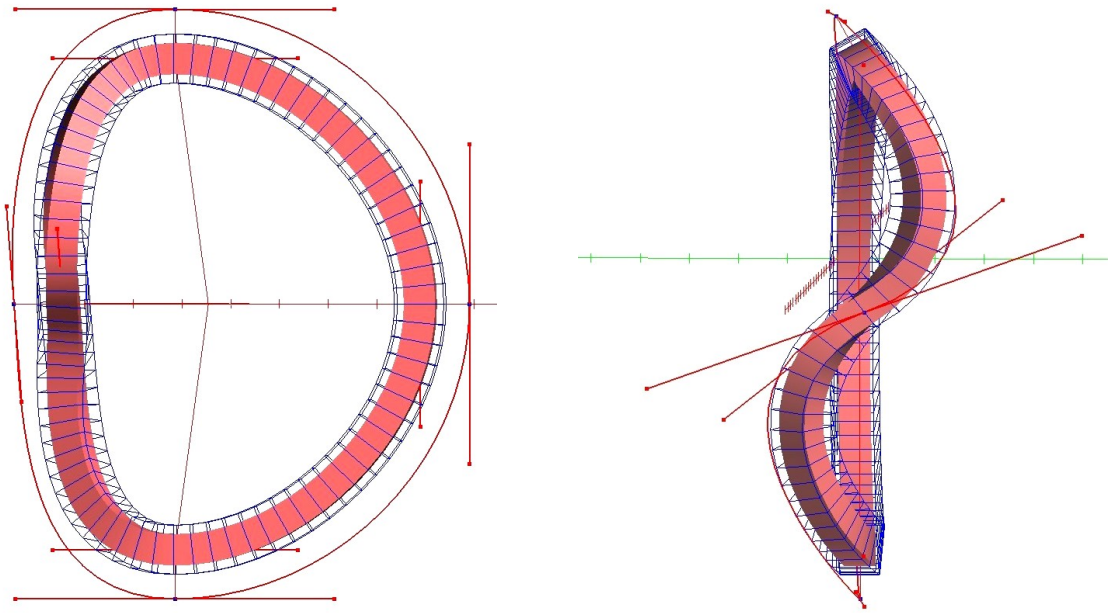

Figure 3: Two aspects of a non-planar D-shaped coil

2.2 Coil cross section

In most stellarators the shape of the coil cross section is a rectangle with width w and height h and we can model the 4 boundary curves of the winding pack or the coil casing by

$$\boldsymbol{Z}_i = \boldsymbol{Y}_i \pm \frac{h}{2}\boldsymbol{n}_i \pm \frac{w}{2}\boldsymbol{b}_i \quad ; \quad i = 1, ..., N. \tag{2}$$

Here, $\boldsymbol{n}_i$ and $\boldsymbol{b}_i$ are the normal and binormal vectors of the coil. Since reactor coils must keep the current density as small as possible, a trapezoidal cross section of the winding pack is favourable. For this reason, on the high-field side of the coil the width is larger than on the low field side. The purpose is to make the force density in the coil as small as possible. The two boundary curves on the high-field side of the coil are

$$\boldsymbol{Z}_i = \boldsymbol{Y}_i - \frac{h}{2}\boldsymbol{n}_i \pm \frac{w_i}{2}\boldsymbol{b}_i \quad ; \quad i = 1, ..., N \tag{3}$$

and on the low field side

$$\boldsymbol{Z}_i = \boldsymbol{Y}_i + \frac{h}{2}\boldsymbol{n}_i \pm \frac{w_a}{2}\boldsymbol{b}_i \quad ; \quad i = 1, ..., N \tag{4}$$

with $w_i \geq w_a$. Fig.6 displays the trapezoidal cross section of a reactor coil consisting of a coil casing, an insulation and superconducting cables. The choice of the superconductor is dictated by the highest magnetic field in the coil. As will be shown later this is in the range of 10 T while the average magnetic field in the plasma is 5 T. In principle a $NbTi$-superconductor could be used, however the cooling temperature must be kept below 1.8 K. During the design phase of Wendelstein 7-X a modular coil based on this technique has been succesfully tested at the Kernforschungszentrum Karlsruhe. The magnetic field could be raised to 11 T.

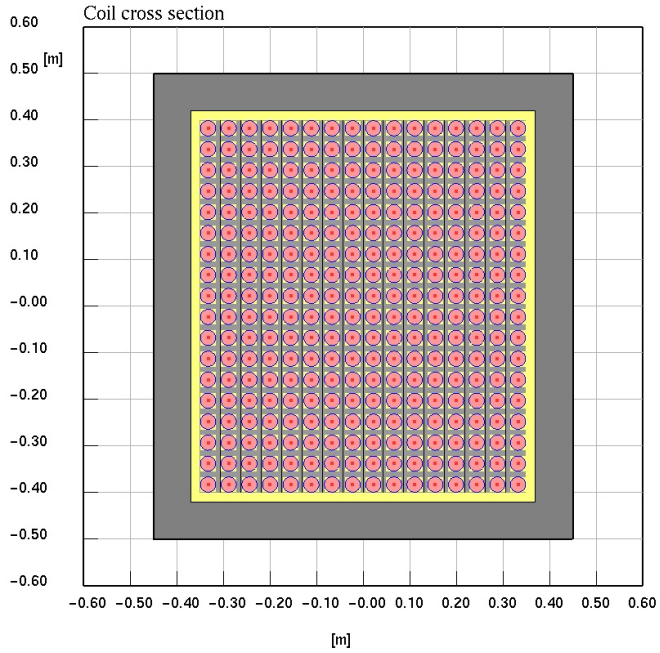

Figure 4: Rectangular cross section of a reactor-size coil with a casing and a winding pack. The size of the casing is 1.0 x 0.9 m^2, the number of turns is 288. Diameter of cable 33 mm, current 42 kA, $NbTi$-cable

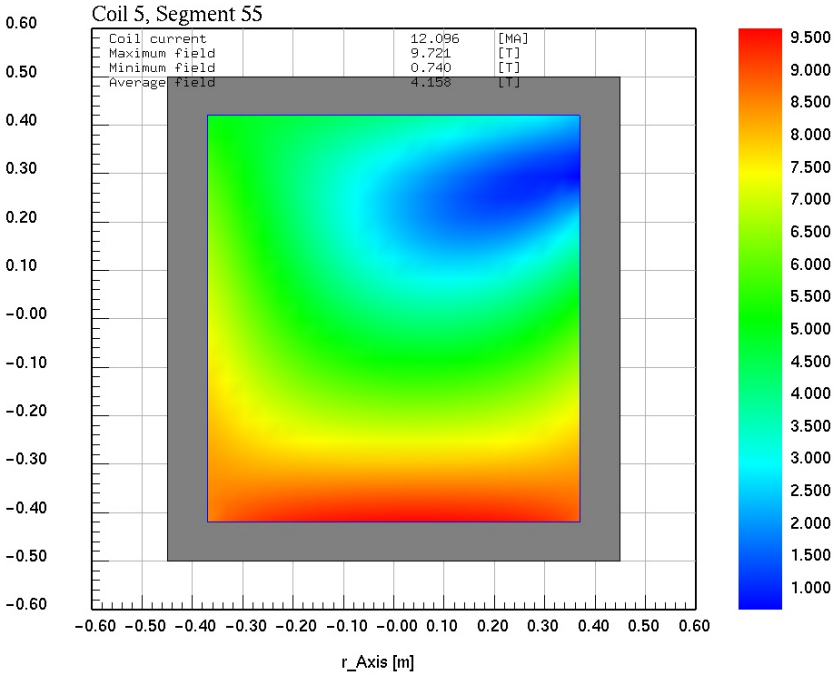

Figure 5: ModB in coil cross section. The color scale shows modB in Tesla. The maximum field is 9.7 T

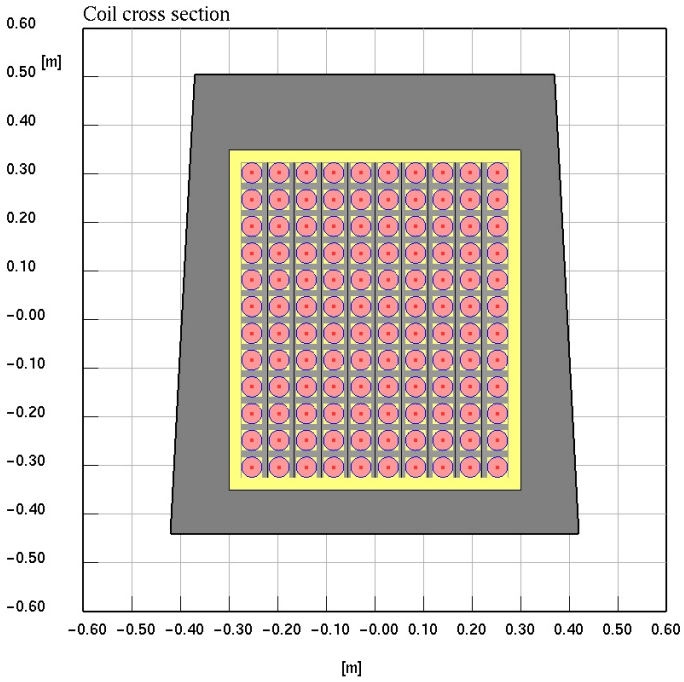

Figure 6: Trapezoidal cross section of a reactor-size coil with a casing and a winding pack. The number of turns is 120. Diameter of cable 42 mm, current 112 kA, Nb_3Al-cable

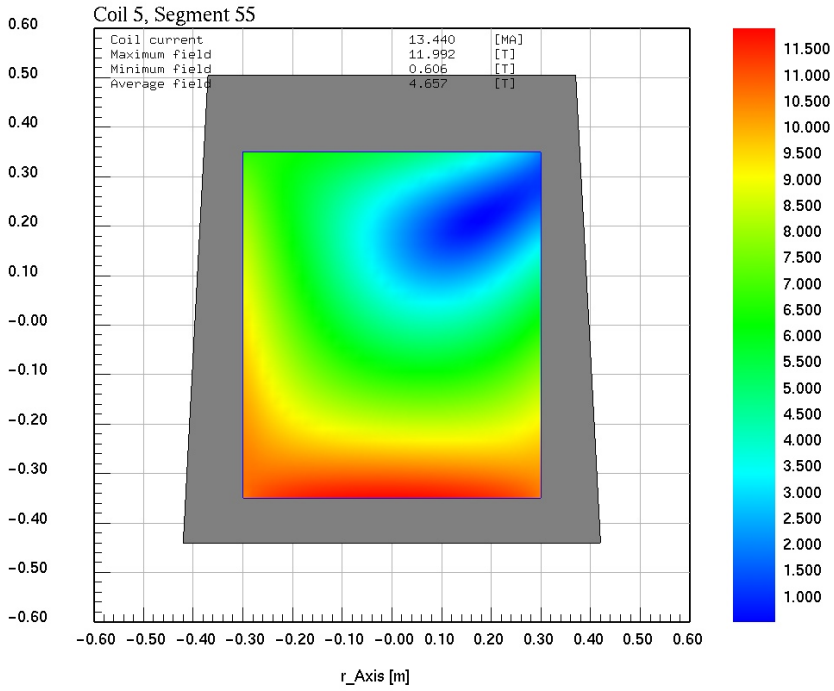

Figure 7: ModB in coil crosssection. The color scale shows modB in Tesla. The maximum field is 12 T

A Nb_3Sn-cable, as envisaged for ITER, allows higher magnetic fields, however the wind-and-react-technique may turn out to be a problem in non-planar coils. In future, Nb_3Al-cable may be an alternative which avoids this technique. Furthermore, higher magnetic fields and cooling

temperatures are possible. Figure 6 displays a coil cross-section based on a Nb_3Al-cable. As compared with a $NbTi$-cable (Fig.4) a smaller number of turns leads to a smaller cross-section of the winding pack.

Computing the magnetic field of modular coils requires different methods according to the specific purpose. In order to compute field lines and magnetic surfaces in the plasma region a Biot-Savart approach is sufficient, where the coils are represented by the central filament. The magnetic field inside the coils requires more elaborate methods taking into account the finite size of the coils. The highest magnetic field exists on the inner boundary of the winding pack, which determines the choice of the superconductor. A rough overview can be found by the EFFI-approach [**?**], where the winding pack is decomposed in a set of straight rectangular beams and the magnetic field of these segments is given in terms of analytic functions. This procedure, however, does not apply to a coil with trapezoidal cross-section; here more elaborate methods need to be developed.

3 The classical stellarator

The classical stellarator is a configuration where the helicity of magnetic field lines is generated by a system of toroidal field coils and helical windings. Examples of a classical stellarator are Wendelstein 2-A, Wendelstein 2-B and Wendelstein 7-A. In Heliotron-J, LHD and other helical systems the continuous helical coils are the main components of the magnet system. Replacing this coil system by a system of modular coils was the main result of a paper by Wobig and Rehker [**?**]. The next figure 8 shows a 4-period modular stellarator which replaces a classical $m = 4, \ell = 2$-stellarator. The coils are modelled according to the procedure described above and all coils have equal shape. The rotational transform is achieved by a poloidal rotation of each coil relative to its neighbours. Each coil is described by four cubic segments. The rotational transform is rather small, however it can be easily modified by varying the minor radius of the coils or the toroidal elongation.

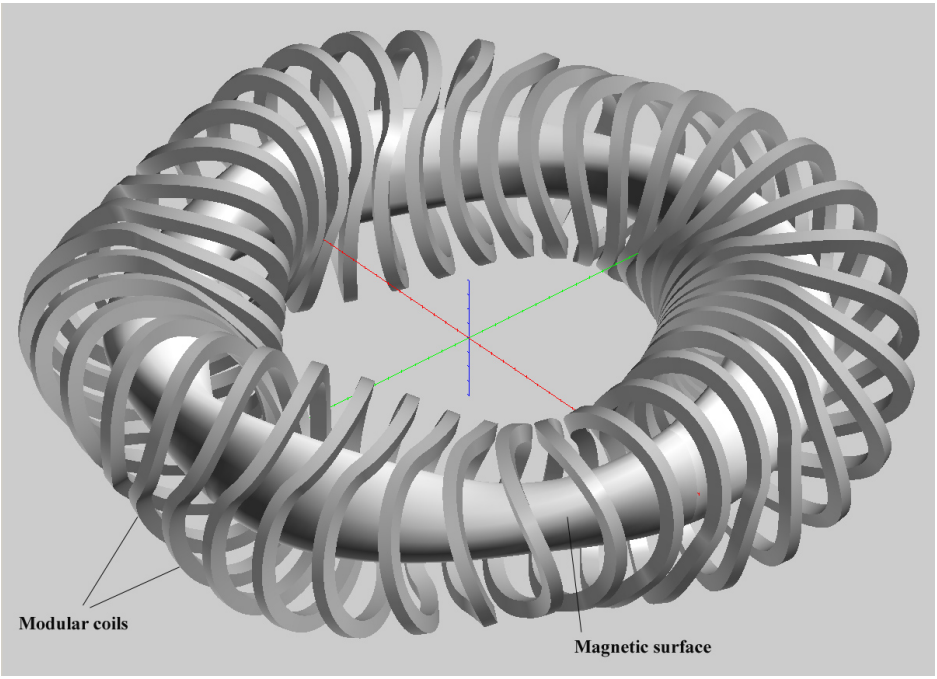

Figure 8: Modular stellarator with 4 field periods. All coils are identical but rotated by different poloidal angles. The rotational transform is $\iota = 0.18$, the shear is near zero.

4 The Helias reactor

Wendelstein 7-X is a modular stellarator experiment under construction in Greifswald, Germany. The magnetic field is optimized with respect to the plasma equilibrium, stability and neoclassical confinement. Reactor prospects of this configuration have been investigated and published on various occasions [**?**],[**?**]. A Helias reactor of the Wendelstein 7-X-type is roughly 4 times larger than the experiment, the main criterion for defining the dimensions is to provide enough space for blanket and shield. The following section describes the analytic approximation of the Wendelstein 7-X coils and a computation of the magnetic field for this approximation. It turns out that five cubic segments are needed to represent the modular coils of Wendelstein 7-X. In this approach the approximation is made interactively on the PC, a systematic procedure may provide a better approximation. The following figure 9 shows the central filaments of Wendelstein 7-X and its analytic approximation in reactor size (R=22 m).

The maximum distance between the two curves is of the order of 5-10 cm. This leads to small deviations from the original Wendelstein 7-X configuration however, since the 5-fold symmetry is preserved, this is a tolerable effect. The central filament is used to compute the magnetic field in the plasma region with the help of Biot-Savart's law.

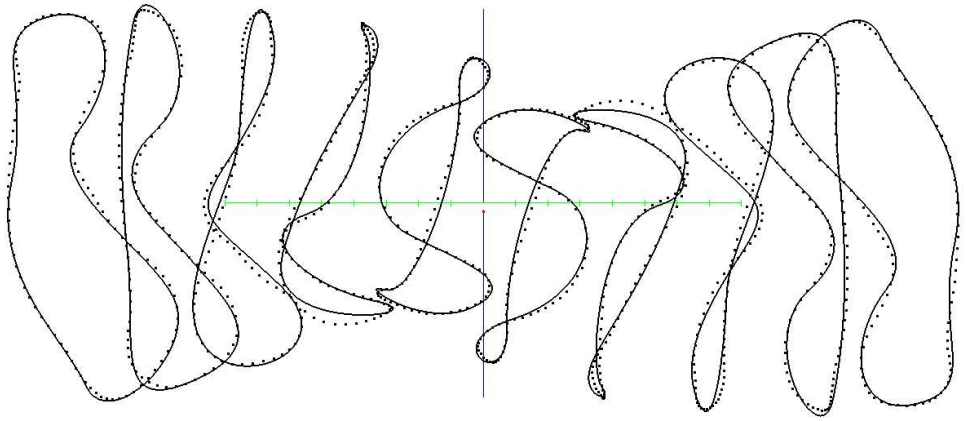

Figure 9: Central filaments of Wendelstein 7-X coils (black dots) and the analytic approximations (solid lines). One period.

Keeping the shape of the Wendelstein 7-X coils invariant, several configurations have been studied. This comprises also configurations with four and three periods. The variable parameters are: major radius, effective radius of the coils and the number of periods. Variation of the effective coil radius means multiplication of all geometric data of the coil with a scaling factor fc.

4.1 Configuration HSR5M

HSR5M is basically a Wendelstein 7-X configuration scaled up by a factor of four. The coil cross section has been designed according to reactor conditions. The finite size coils are shown in the next figures 10 and 11.

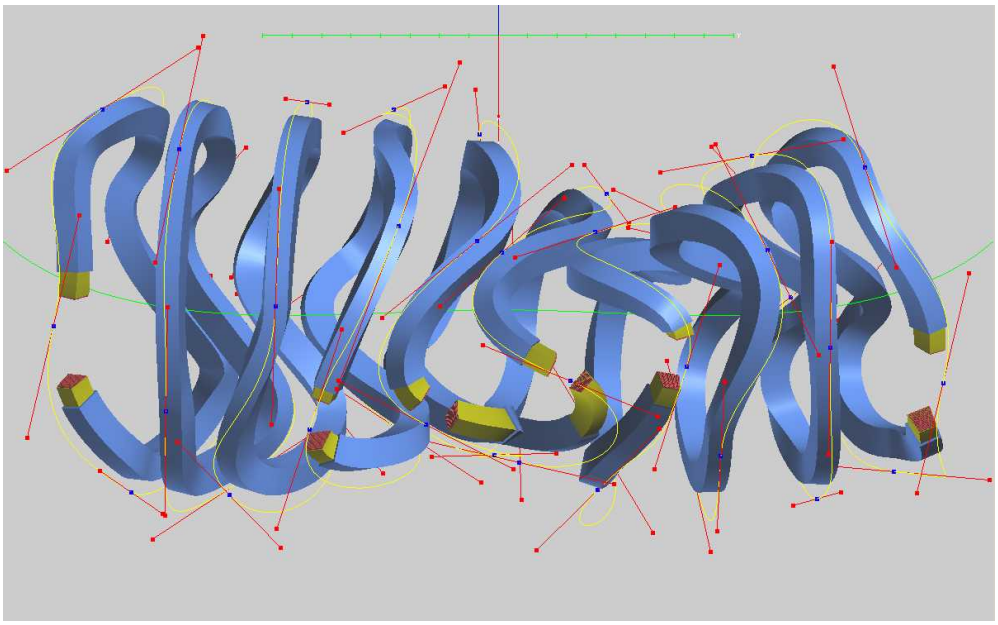

Figure 10: Reactor-size Wendelstein 7-X coils in analytic approximation. One period. Average major radius 22 m. The coil cross section is shown in Fig.**??**

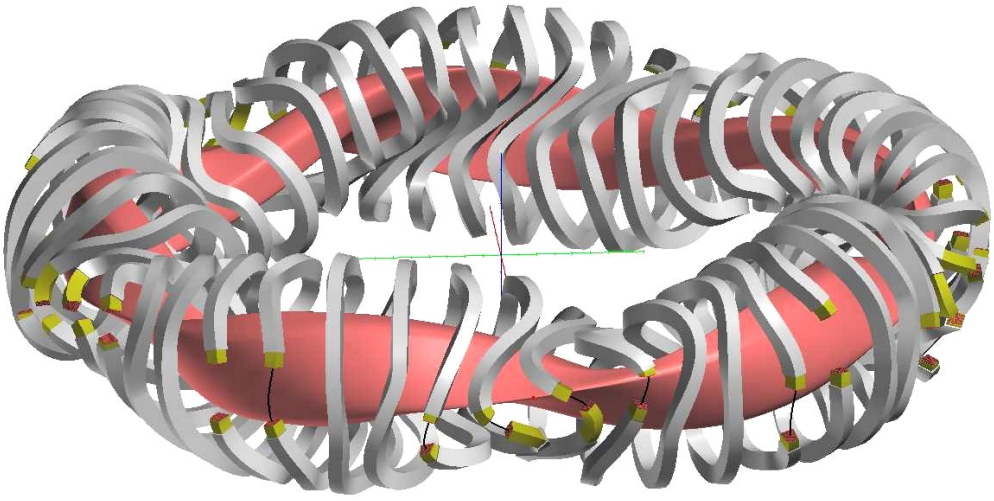

Figure 11: Magnetic surface and coil system of a 5-period Helias configuration HSR5M. Average radius of the last closed magnetic surface: 1.9 m, volume: 1600 m^3.

Table 1: Main parameters of modular coils in HSR5M

Coil	1	2	3	4	5
Casing :					
Height [m] :	1.0	1.0	1.0	1.0	1.0
Width 1 [m] :	1.0	1.0	1.0	1.0	1.0
Width 2 [m]:	0.8	0.8	0.8	0.8	0.8
Cross section [m^2]:	0.9	0.9	0.9	0.9	0.9
Length of coil [m] :	34.18	33.88	33.61	34.19	34.46
Spec. weight [tm^{-3}]	7.8	7.8	7.8	7.8	7.8
Volume [m^3]:	30.76	30.49	30.25	30.77	31.01
Weight (steel)[t]	239.9	237.8	235.9	240.0	241.9
Cable :					
Width of cable [m]:	0.033	0.033	0.033	0.033	0.033
Current in cable [kA]	42.0	42.0	42.0	42.0	42.0
Number of turns	288	288	288	288	288
Length of cable [m]	9844	9758	9681	9848	9926
Current [MA turns]	12.1	12.1	12.1	12.1	12.1
Vol. of cable [m^3]	10.72	10.62		10.72	10.81

The current in the cable is 42 kA and the number of turns is 288. This leads to an average magnetic field of 5 T on the magnetic axis. The weight of the coil is about 240 t if it consists of steel only. This is an upper limit, depending on the amount of SC cable and insulation, the real weight is smaller. Magnetic field surfaces of HSR5M configuration are represented in Fig. 12. The color clearly displays the modular ripple which gives rise to locally trapped particles.

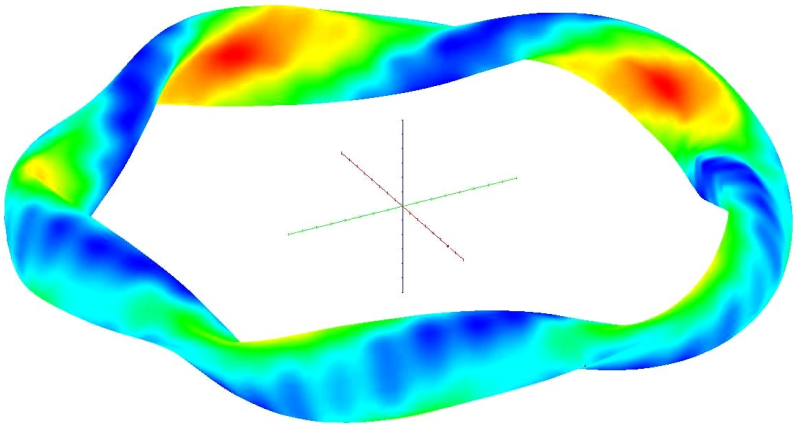

Figure 12: Magnetic surface of a 5-period Helias configuration HSR5M. The color indicates the magnetic field strength on the surface. Average radius of the last surface: 1.9 m, volume: 1600 m^3.

The rotational transform at the edge is unity and 5 islands on this rational surface limit the confinement region. As in Wendelstein 7-X, these islands can be utilized for divertor action.

4.2 Comparison with Wendelstein 7-X

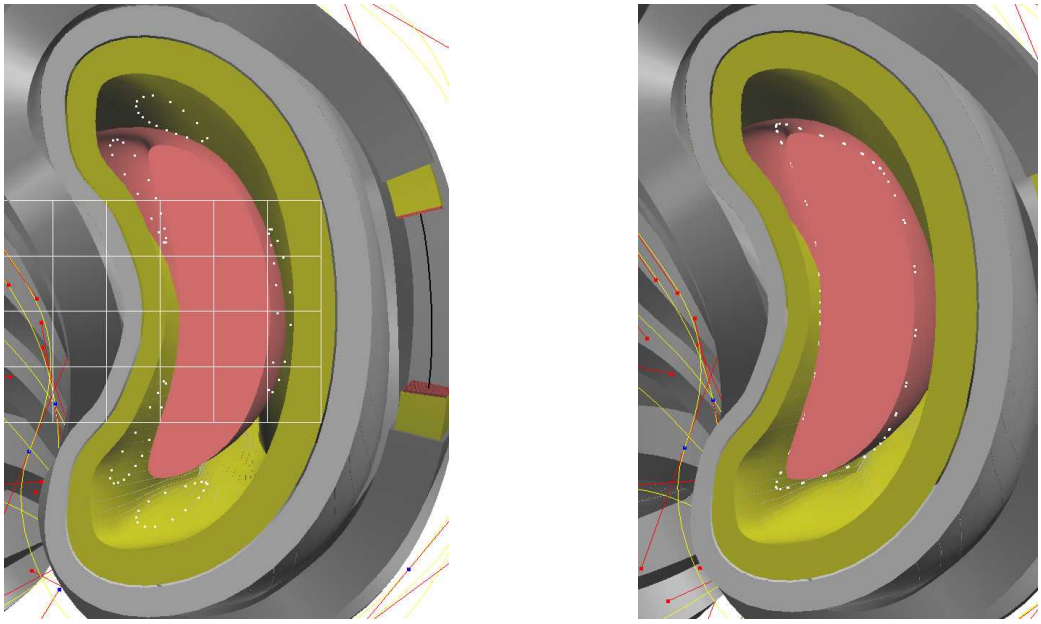

Figure 13: Left: 5 islands on the $\iota = 1$-surface. Scale 1m. Right: Comparison of a Wendelstein 7-X-surface (red) with a surface of the reactor coil system (white spots)

As can be seen in fig. (**??**) the central filaments of Wendelstein 7-X and the cubic approximation (solid lines) differ slightly. The impact on magnetic surfaces is demonstrated in the next figures.

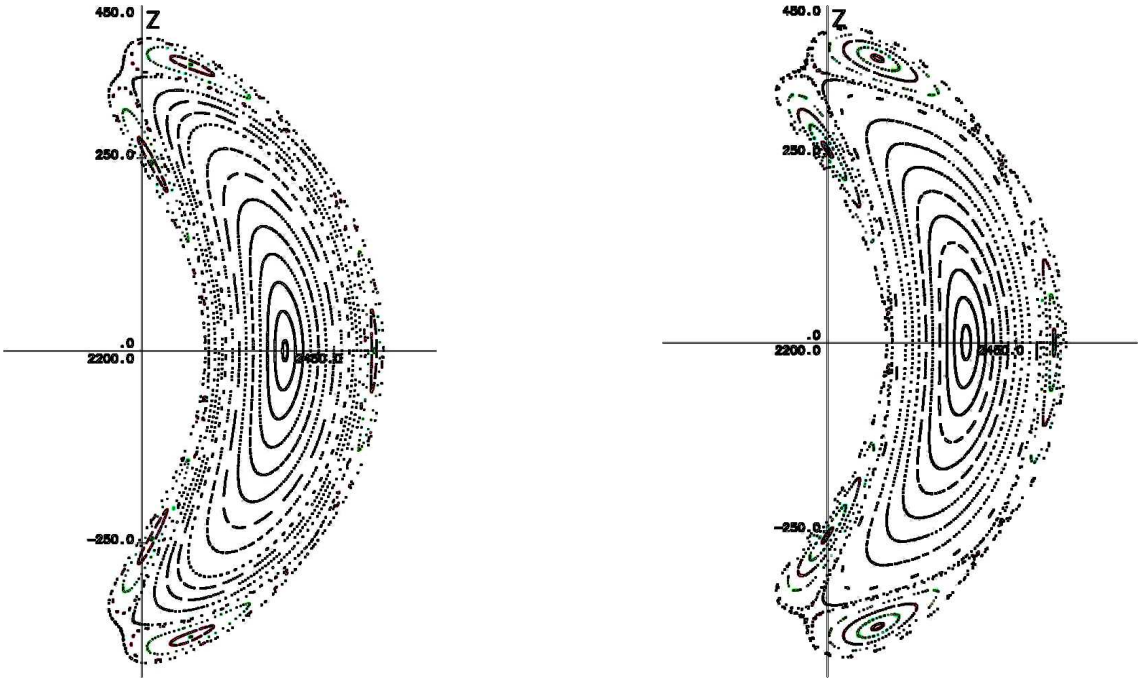

Figure 14: Left: Poincaré plot of Wendelstein 7-X. Right: Cubic appproximation of central filaments

The main difference between Wendelstein 7-X and its approximation HSR5M is the size of the islands on the boundary, the difference of closed magnetic surfaces is insignificant. The rotational transform on the axis is $\iota = 0.856$ in Wendelstein 7-X and $\iota(0) = 0.88$ in HSR5M as shown in figure 15.

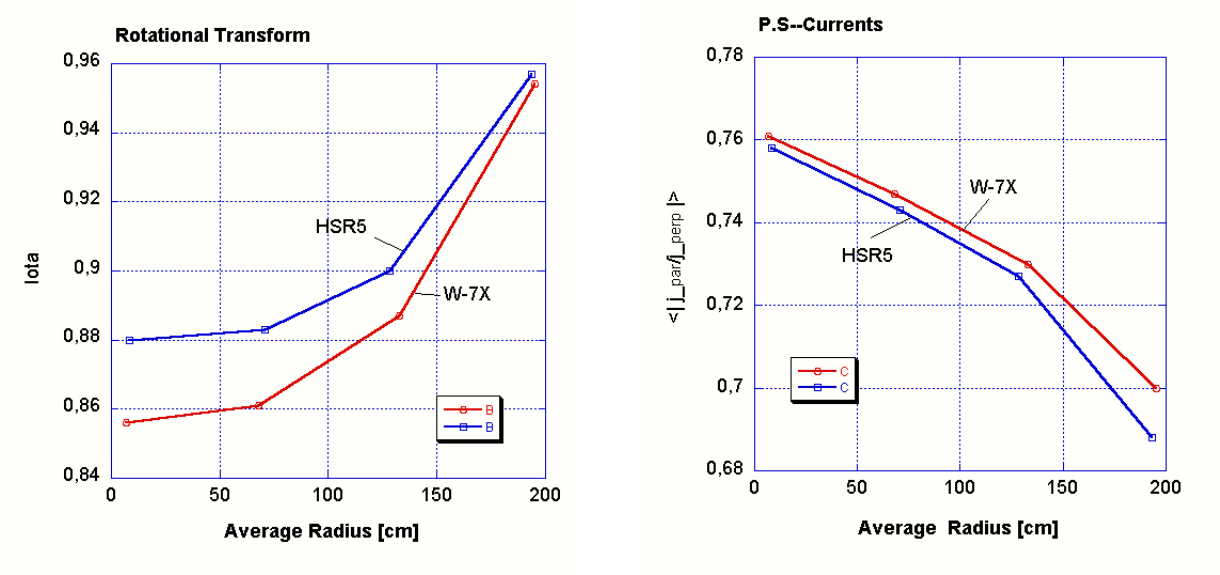

Figure 15: Left: Rotational transform. Right: Pfirsch-Schlüter currents/diag. currents. W7-X dimensions are multiplied by 4.

A basic feature of Wendelstein 7-X is the reduction of Pfirsch-Schlüter currents and the reduction of the Shafranov shift. This optimized property is nearly unaltered by the cubic approximation of the central filaments. The averaged ratio of the parallel current density to the diamagnetic current density is a figure of merit for the degree of optimisation. Figure 15 shows only a minor difference in the P.S-currents, the deviation of the central filaments from the filaments in Wendelstein 7-X has only a small impact on the degree of optimisation. The degree of optimisation, the reduction of P.S.-currents is even larger in HSR5 than in Wendelstein 7-X. In both cases the averaged P.S.-currents are smaller than the diamagnetic currents. Another figure of merit for optimised stellarators is the magnetic well which is about 1% in both cases.

4.3 The 5-period configuration HSR515M

HSR515M is a configuration where the average radius of the coils has been increased by 1.5% while the major radius of the coil system has been kept at 22 m. The effect on the last closed magnetic surface and the plasma volume is stronger than 1.5%, the effective plasma radius grows to more than 2 m and the volume of the last closed surface is 1800 m^3. This demonstrates that small changes of the coil system may have a strong effect on magnetic surfaces. However, since the average radius of the coils grows only slightly the availlable space for the blanket shrinks. In a second example the average radius of the coils has been reduced by 1% (HSR599) which also reduces the effective plasma radius. The Poincaré plot of the magnetic surfaces is shown in the next figures.

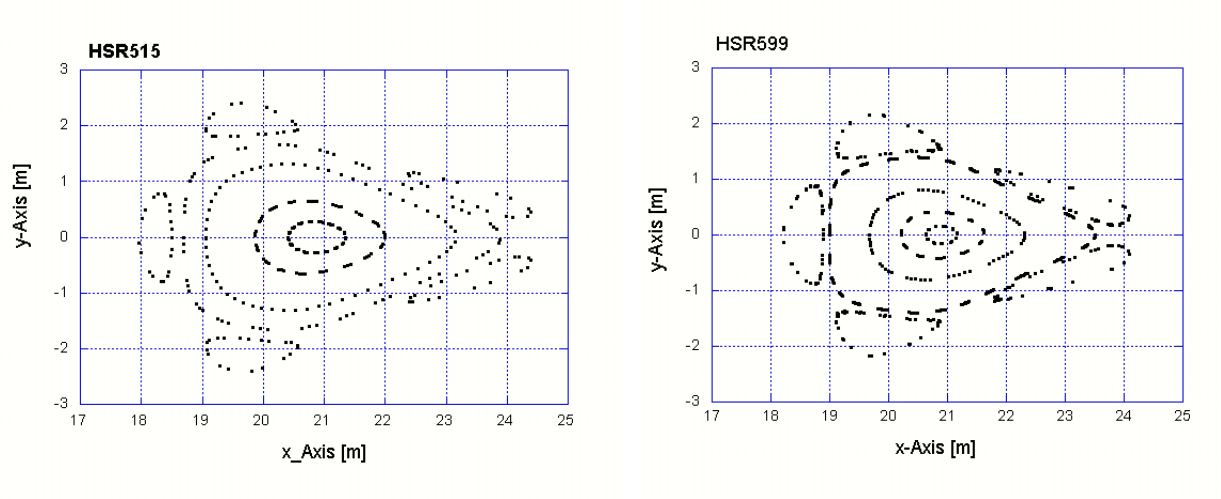

Figure 16: Left: HSR515M, factor $fc = 1.015$. Right: HSR599M, factor $fc = 0.99$

In all these cases the rotational transform at the edge is $\iota = 1.0$. The islands at the edge are independent, they are not connected and symmetry-breaking perturbations of the coil system may lead to strong asymmetries of the islands. This prevents an effective divertor action and for this reason systems with 4 and 3 field periods are of interest and will be discussed in the next sections. Furthermore, the reduction of field periods and major radius leads to smaller and less expensive devices.

4.4 The 4-period configuration HSR4M

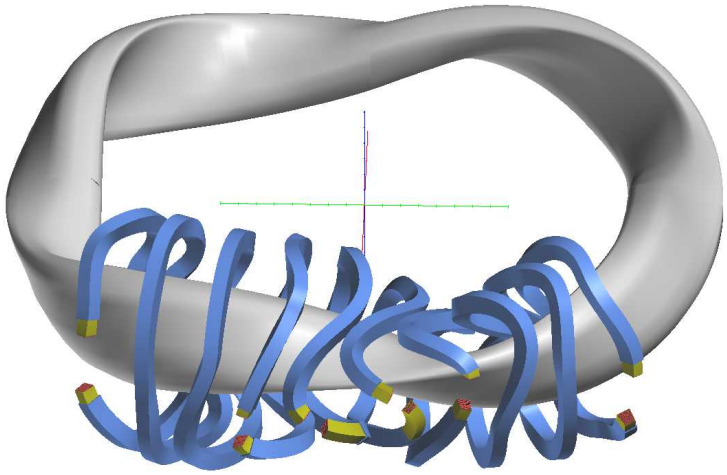

Figure 17: Magnetic surface of a 4-period Helias configuration HSR42M. Average radius of the last surface: 1.95 m, volume: 1656 m^3, ι=0.774

The 4-period Helias coil system HSR4M consists of 40 modular coils and the average major radius is 18 m. The cross section and the shape of the coils is the same as in HSR5M (see fig. **??**).In the example HSR41M the coils are the same as in HSR5M, in a second example HSR42M the coils have been scaled up by 4% keeping the shape and the cross section invariant.

Increasing the coils by 4% (HSR42) leads to a significant growth of the magnetic surface. The average plasma radius (radius of last surface) becomes 1.95 m, while in HSR41 the average radius is only 1.5 m.

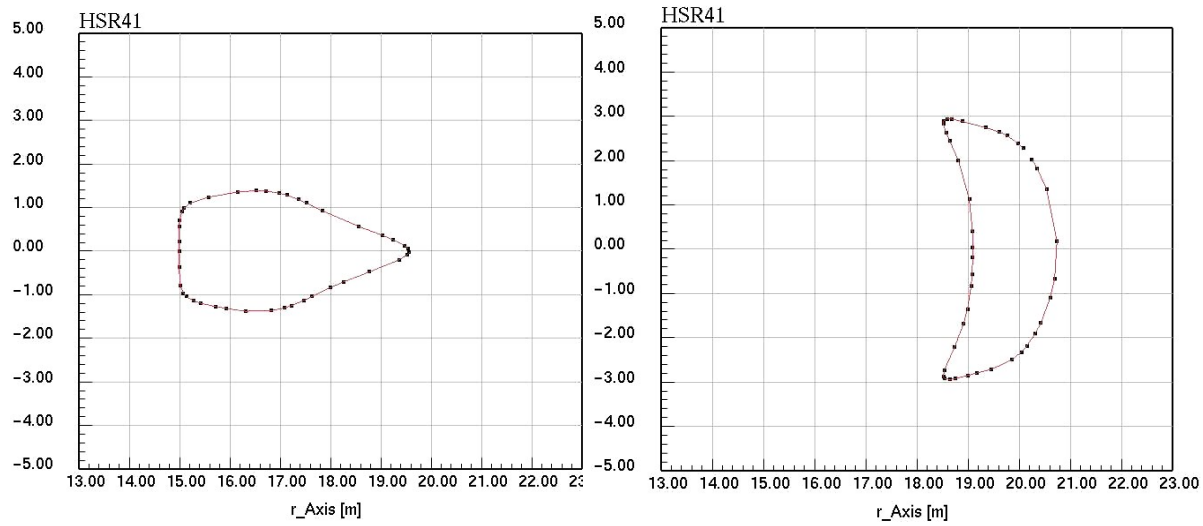

Figure 18: Poincaré plot of last magnetic surface in HSR41M

Magnetic surfaces and one period of the coil system HSR42 are shown in the next figures. Beyond the last magnetic surface 5 islands exist located on the rational surface with ι=4/5=0.8. In fact, this is only one island which makes 5 toroidal turns and 4 poloidal ones before closing upon itself.

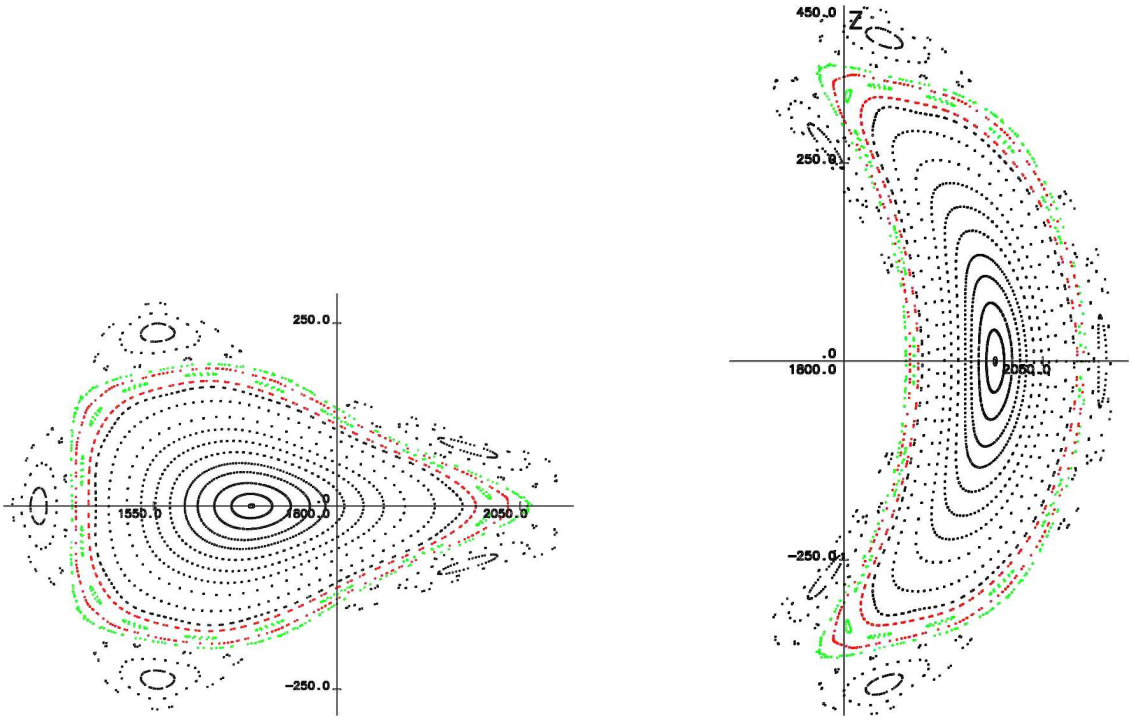

Figure 19: Poincaré plot of magnetic surfaces in HSR42M

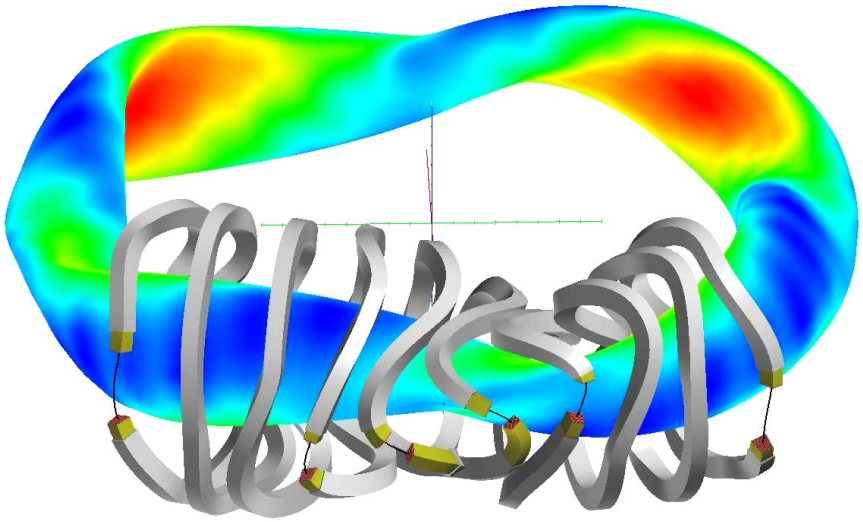

Figure 20: Magnetic surface and modB of a 4-period Helias configuration HSR42M. Average radius of the last surface: 1.95 m, volume: 1656 m^3, ι=0.773

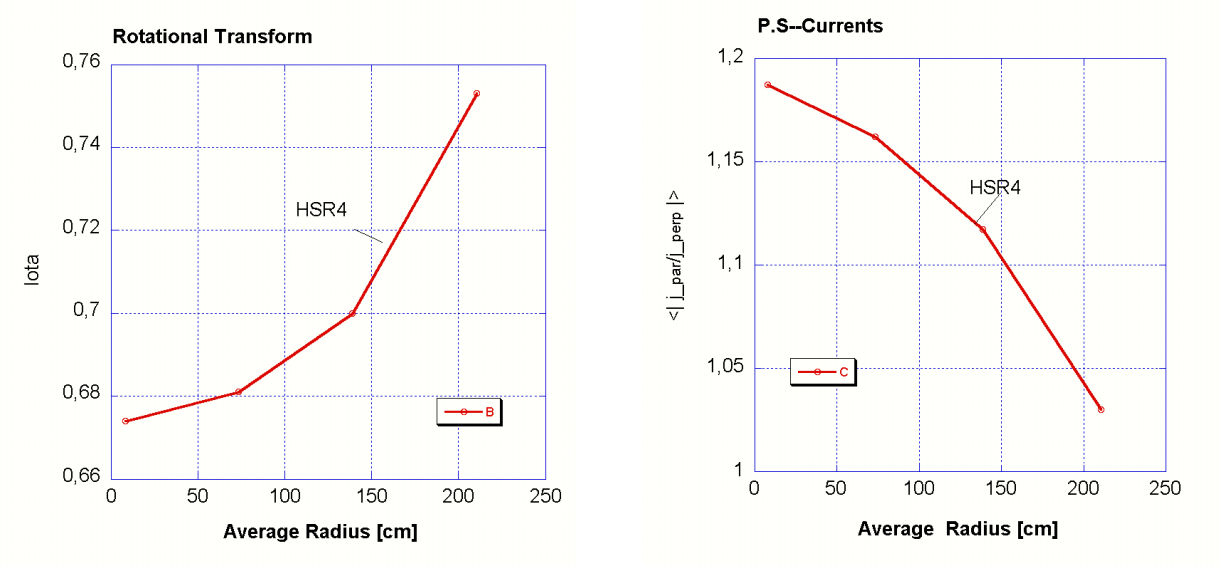

Figure 21: Left:HSR4M, Rotational transform. Right: Pfirsch-Schlüter currents/diag. currents

The Pfirsch-Schlüter currents are larger than in case of 5 field periods (HSR5M). The reason is the reduction of the rotational transform which certainly will result in a higher Shafranov shift. The rotational transform at the edge is 0.8. There are 5 islands, however these are connected and any symmetry-breaking perturbation affects all islands. This will cause a stochastisation of the island region.

4.5 The 3-period configuration HSR3M

HSR3M is a third configration with 3 field periods and 30 modular coils. The average major radius is 15 m and the Wendelstein 7-X coils have been multiplied by a factor of 4.4, which is 1.1 times larger than in HSR5M. The purpose of this increase is to provide a sufficiently large plasma volume.

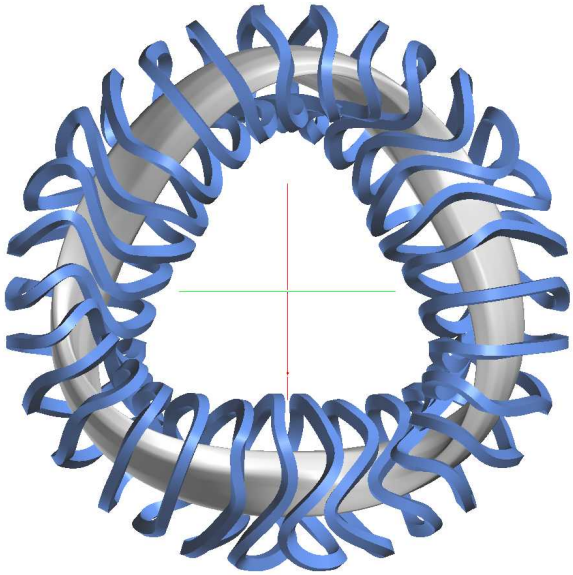

Figure 22: Magnetic surface of a 3-period Helias configuration HSR3M. Average radius of the surface: 1.52 m, volume: 1007 m^3, ι=0.538.

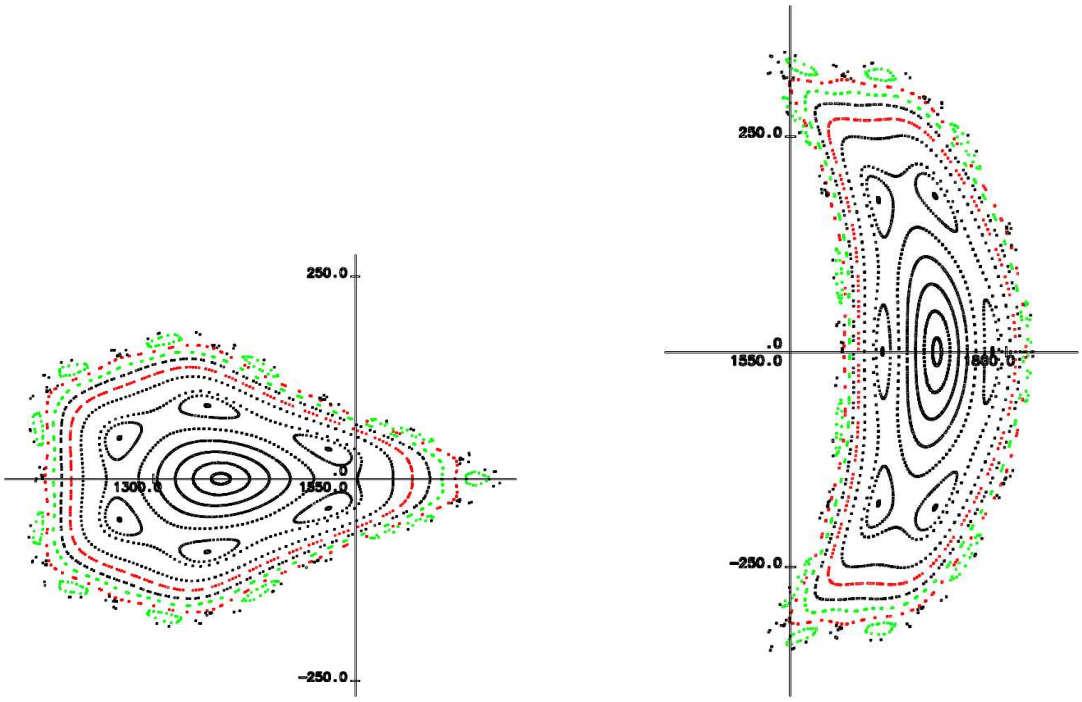

Figure 23: Poincare plot of magnetic surfaces in HSR3M.

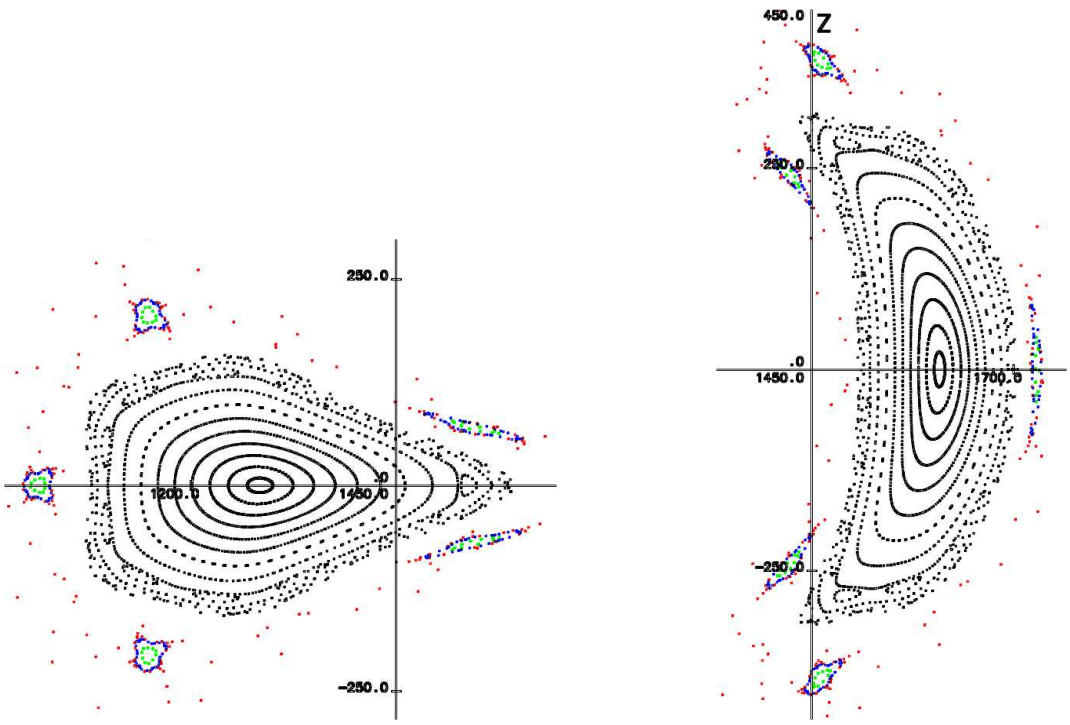

Figure 24: Poincare plot of last magnetic surface in HSR32M. Av. radius of last surface 1.5 m, rot. transform ι=0.565

In configuration HSR3M a low-order rational surface with $\iota = 0.5$ exists which exhibits 6 islands. In order to avoid this situation the parameters have been changed slightly. HSR32M has a major radius of 14 m and the average radius of the coils has been enlarged by 4%. This modification raises the rotational transform leading to a transform between 0.5 and 0.6 (fig. **??**). At the edge the remnants of the $\iota = 0.6$-islands can be utilized for divertor action. As in configuration HSR4 the islands at the edge are connected and a periodical asymmetry of the coil system modifies all islands simultaneously and does not create asymmetries of the islands.

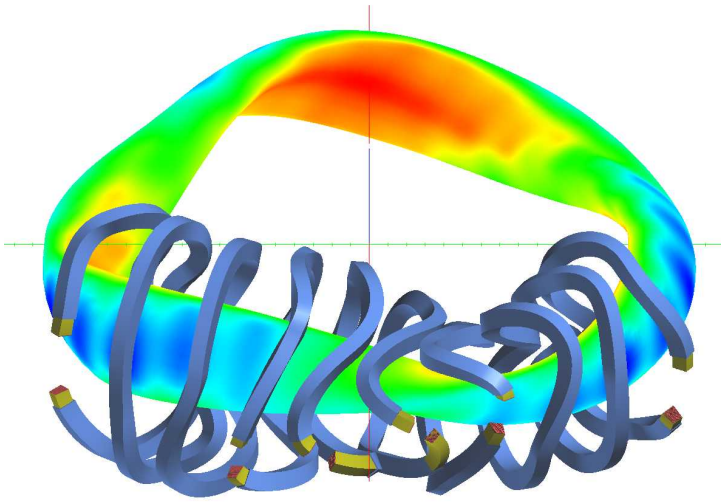

Figure 25: Magnetic surface and modB of a 3-period Helias configuration HSR3M.

4.6 Magnetic field and forces

As input for force and stress analysis the magnetic field inside the coils must be computed. As mentioned above the trapezoidal coil will be approximated by a system of rectangular beams where an analytic formulation of the field is available [**?**]. In the present example the number of rectangular segments is 100. The following figure 26 displays the field strength in the midplane of such a rectangular segment.

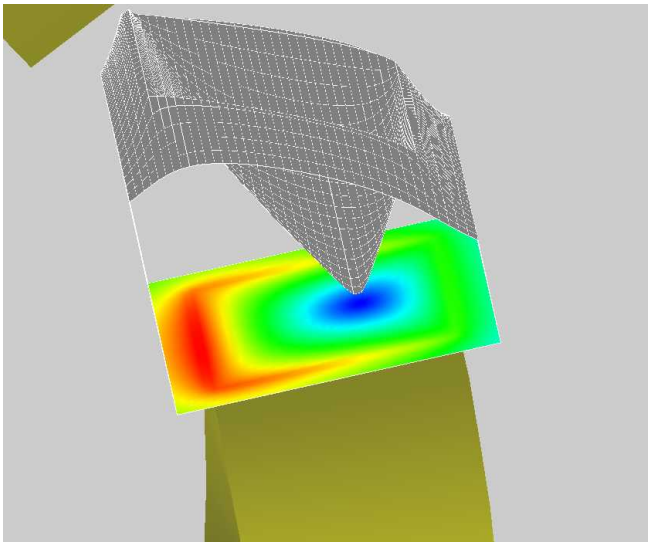

Figure 26: HSR5M: Magnetic field strength in the midplane of segment 1, coil1. Red: high field, blue: low field.

In HSR5M the maximum magnetic field exists in coil 5, segment 55, as shown in figure **??**. The maximum field is 9.7 T and the average field in this plane is 4.16 T. Since the current density in the coil plane is constant the average magnetic field is proportional to the force per length on the coil. In segment 55 this force is 50.3 MN/m. It turns out that the average field is nearly equal to the field on the central filament. Thus, to get a rough estimate of the integrated force per meter, the magnetic field at the central filament is sufficient.

Due to the 3-dimensional shape of the coils the out-of-plane forces may become as large as the forces in the direction of the coil normal vector. The forces per m in coil 5 are shown in the next figures (**??**).

These numbers apply to the coil system with $NbTi$-cable where the magnetic field in the coil stays below 10 T. As described above an Nb_3Al cable allows an increase of the magnetic field in the plasma to 5.5 T and in the coil to 12 T. In order to run a $NbTi$-cable at 10 T super-cooling at 1.8 K is needed. With Nb_3Al cable, however, this restriction is removed and cooling at 4.2 K or higher is possible. On the other hand, raising the magnetic field will increase the issue of forces and stresses inside the coils.

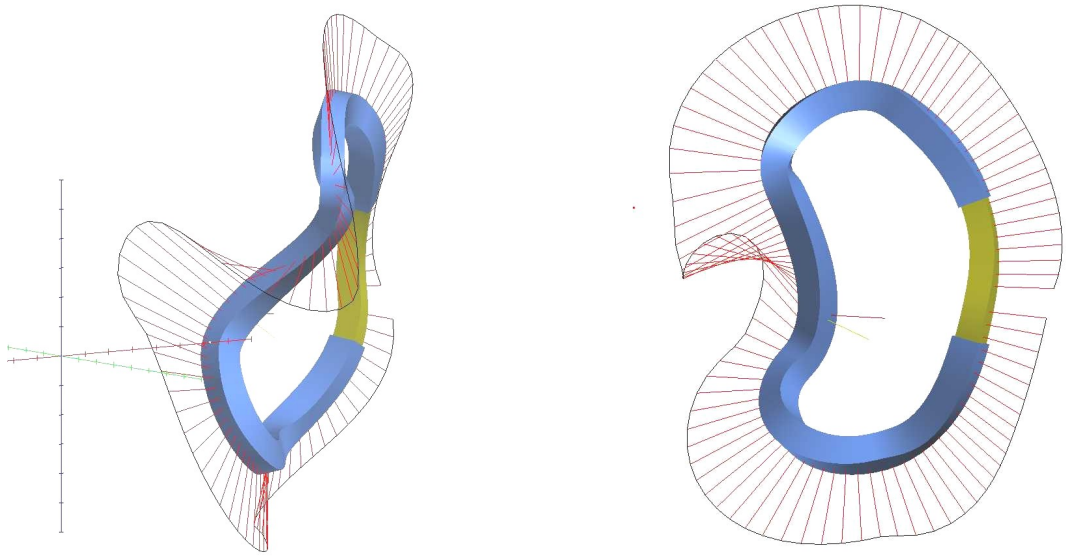

Figure 27: Magnetic forces in coil 5 of HSR5M. The maximum force is 50.25 MN/m.

These results are characteristic for all coils, there is no large difference with respect to forces.

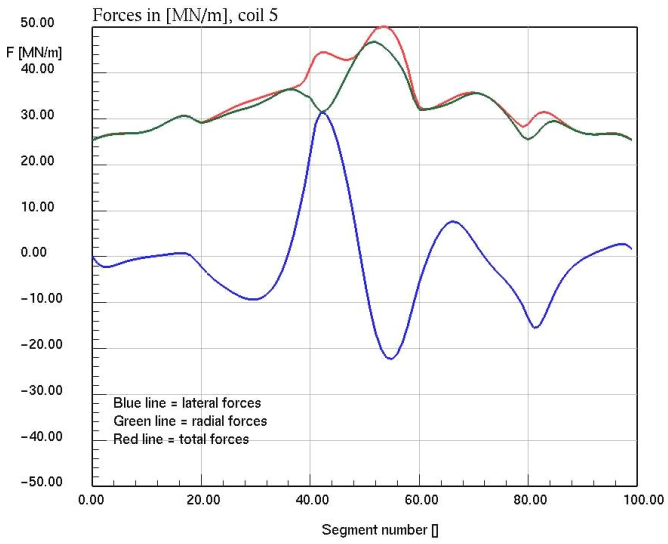

Figure 28: HSR5M: Coil 5, normal forces, lateral forces and total forces per m. The abcissa is the index of the segment

As discussed above, the use of $Nb-Al$-conductors allows one to raise the magnetic field by 10% in the plasma. This implies an increase of the forces by at least 20%. However, since the coil cross section is more compact and the maximum field in the coil is 12 T instead of 10 T the forces will grow by more than 30%. The implication on the support structure and the stress analysis needs further investigations.

5 Summary and conclusions

In this paper it has been shown that modular coils of stellarators can be described by segments of cubic Bézier curves. In case of standard stellarators 4 segments are sufficient, however, modular coils of the type Wendelstein 7-X need 5 segments. By adjusting the control parameters of the segments to the geometry of the Wendelstein 7-X coils a representation of these coils by cubic Bézier curves can be found. The difference between the approximation and the real Wendelstein 7-X-coils remains at a tolerable level; detailed comparison of the magnetic surfaces showed that the optimised properties of the Wendelstein 7-X-concept are maintained. This representation of the coils is the starting point for several reactor configurations with 5, 4 and 3 field periods. In all cases the coils are 4 - 4.4 times larger than the Wendelstein 7-X coils, the shape, however, is kept invariant. A scaling factor is introduced to modify the coils independently of the major radius. The following table displays the main parameters of Helias reactors with Wendelstein 7-X-like coils.

Table 2: Main parameters of Helias reactors

HSR	5M	41M	42M	3M	31M	32M
Av.major radius [m]	22	18	18	15	13.5	14.0
Number of periods	5	4	4	3	3	3
Number of coils	50	40	40	30	30	30
Scaling factor f_c	1	1	1.04	1.1	1.05	1.04
Radius of last surface [m]	1.86	1.5	1.95	1.52	1.56	1.49
Volume of last surface [m^3]	1516	986	1656	1007	1057	970
Iota of LCMS	0.976	0.77	0.774	0.538	0.559	0.565
Iota of islands	1.0	0.8	0.8	0.6	0.6	0.6

The factor f_c is the scaling factor of the coil, linear dimensions of the coil - exept the cross section - are multiplied by f_c. The total current in the coil is 12.1 MA, which provides a magnetic field of 5 T on the magnetic axis in all cases. The magnetic field inside the coil winding pack stays below 10 T in all configurations, which leads to rather moderate forces on the coils. The maximum force per unit length is 50 MN/m. Because of the 3-dimensional shape of the coils the lateral forces are of the order of the radial forces, which provides a challenge to the coil support system.

As an alternative to the $NbTi$-conductor a Nb_3Al-conductor has been considered. This allows raising the magnetic field in the coils to about 13 T and to operate at cooling temperatures of 4.2 K or more. An example is given where the magnetic field in the plasma is 5.5 T and 12 T on the coils.

Since the magnetic configuration of HSR5M is the same as in Wendelstein 7-X, all theoretical results of Wendelstein 7-X, which are scale-invariant, are also applicable to HSR5M. In particular, this applies to the MHD-equilibrium and MHD-stability limits, as well as to neoclassical transport and neoclassical bootstrap currents. The small difference in rotational transform may be insignificant. Because of its compactness the smaller Helias reactor HSR3M is an attractive alternative, here however, plasma physics properties need to be optimized.

The code MODUCO provides an easy-to-handle and convenient tool to design optimized reactor configurations. Together with magnetic surfaces the code computes the magnetic field inside the coils and thus provides the input data for structural analysis. The maximum field on the coils determines the choice of the superconductions. In the examples described in this paper the magnetic field in the coils stays below 10 T, while the average field in the plasma region is

5 T. The shape of the coils can be optimized interactively according to engineering constraints while the impact on magnetic surfaces and thus on the plasma perfomance can be monitored simultaneously. The code is flexible enough to model any reactor configuration utilizing modular coils.

References

[1] A. Gibson and D.W. Mason, Plasma Phys. vol. 11, p. 212, 1969

[2] H. Wobig and S. Rehker, *A Stellarator Coil System without Helical Windings*, Proc. 7th Symp. on Fusion Technology, Grenoble, France, 333-343 (October 24-27, 1972).

[3] P. Merkel , Nucl. Fusion **27**,5, 867 (1987)

[4] D.J. Strickler, L.A. Berry, S.P.Hirshman, *Designing coils for compact stellarators*, Fusion Science and Technology, 33 (1998) 106

[5] S.J.Sackett, LLNL report UCRL-52402, 1978

[6] H. Wobig et al. *The concept of a Helias ignition experiment*, Nucl. Fusion **43** (2003) 889-898

[7] C.D. Beidler et al. *The Helias reactor 4/18*, Nucl. Fusion **41** (2001) p. 1759